*J. Earth Syst. Sci.* (2022)131 171
https://doi.org/10.1007/s12040-022-01908-y



# On assessing the influence of a newly impounded reservoir on a nearby normal fault using a simple three-dimensional model of subsurface geological heterogeneity

Ramesh Chander[1] and S K Tomar[2,*]

[1]*House No. 290, Sector 4, Mansa Devi Complex, Panchkula 134 114, Haryana, India.*
[2]*Department of Mathematics, Panjab University, Chandigarh 160 014, India.*
**Corresponding author. e-mail: sktomar@pu.ac.in*

MS received 4 April 2021; accepted 22 February 2022

We assume that the subsurface at the site of a newly impounded reservoir has a small volume of rock with porous-elastic properties significantly different from those of the other rocks in the area. A normal fault passes through this rock volume. We adopt the following simplifications to quantify reservoir influence at different points of the fault in such a case. The reservoir is circular and of uniform depth. The small rock volume is spherical in shape and embedded in an otherwise homogeneous half space with values of porous-elastic properties in the range normally observed through laboratory measurements on rocks. We infer from calculated results that the reservoir will promote slip at low water level at points of the fault lying within the small rock volume if its diffusivity, and undrained and drained Poisson's ratios are significantly lower than those of the other rocks at the site. The reservoir will promote slip on the normal fault at points outside the small rock volume at high water level.

**Keywords.** Manmade reservoir; normal faults; induced earthquakes; geological heterogeneity; simulation; rock mechanics.

## 1. Introduction

Towards the end of 1960's, it was generally accepted that the commissioning of a new dam and the associated reservoir may lead to earthquakes in their vicinity (Gupta and Rastogi 1976). Since then, many case histories have been examined and many models of the subsurface have been considered to rationalize the phenomenon. The well-known example of post-impoundment normal-fault earthquakes under Lake Mead provided motivation for this investigation.

## 2. Review of subsurface models considered for post-impoundment earthquakes

Snow (1972) computed stresses and pore pressure induced in a solid half space permeated with water-filled vertical cracks and overlain by an infinite reservoir. He used principles of rock mechanics (e.g., Jaeger and Cook 1969) to shed light on post-impoundment earthquakes.

However, a homogeneous PE (porous-elastic) half space is the most frequently used model of the subsurface for investigating post-impoundment earthquakes. In support of this model, Roeloffs

Published online: 02 August 2022

(1988, p2108) opined that '... before invoking the complications of material heterogeneity... the uniform porous-elastic model should be proved an inadequate description of the phenomenon of induced seismicity'.

Singh and Rani (2006) developed theory for a subsurface with multiple PE layers resting on a PE half space. Chander and Tomar (2016) considered a PE layer embedded in an elastic half space.

We present results for an axially-symmetric three-dimensional model in which a sphere (short for porous-elastic sphere) is embedded in an HS (short for porous-elastic half space) and there is a uniform circular reservoir on its top surface (figure 1). The results presented below were obtained using the computational procedure outlined in Appendix A for purposes of record.

## 3. Observational data

Geological observations had indicated presence of normal faults under the deepest part of Lake Mead. An epicentral map presented by Rogers and Lee (1976) shows a prominent alignment of earthquake epicenters along a line which also passes over the deepest part of the reservoir. Rogers and Lee (1976) also presented several composite fault-plane solutions for earthquakes occurring under the reservoir. Three of the fault-plane solutions showed normal faulting. Each of these fault-plane solutions was associated with a group of earthquakes whose epicenters appear in a cluster along the lineament. The three fault-plane solutions and the epicentral map indicate that many post-impoundment earthquakes under Lake Mead occurred on normal faults. Roeloffs (1988) argued that some of these normal fault earthquakes occurred at or close to the annual minimum reservoir level.

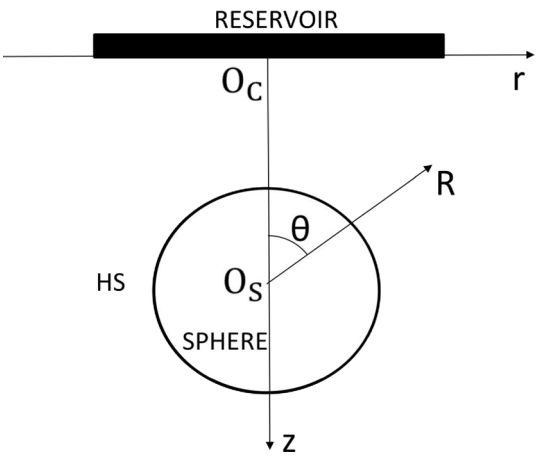


Figure 1. A cross-section of the 3D model with a uniform circular reservoir resting on a porous-elastic half space (HS) with an embedded sphere of a different porous-elastic solid. Also shown are the cylindrical $(r, z)$ and spherical $(R, \theta)$ coordinate systems used.

## 4. Assessing reservoir influence

Figure 1 shows in cross-section the envisaged three-dimensional model of subsurface geology. Cylindrical $(r, z)$ and spherical $(R, \theta)$ coordinate systems needed for locating points in the model are included. Figure 2 shows a rough plane intersecting the sphere. We refer to this plane as 'normal fault' in the following paragraphs. Figure 3 shows the sphere and the fault in a different view (see section 5.1).

The reservoir influence at a point $(R, \theta)$ on the fault may be assessed by comparing the magnitudes of the destabilizing shear stress $\tau_d(R, \theta)$ and the stabilizing frictional stress $\tau_f(R, \theta)$. These stresses are shown schematically in figure 2.

The reservoir influence will promote slip at a point on the normal fault if the magnitude of $\tau_d(R, \theta)$ is greater than the magnitude of $\tau_f(R, \theta)$ and it will favour fault stability in the contrary case.

## 5. Results

The following estimates of destabilizing shear stress and stabilizing frictional stress are for a normal fault dipping at 60° (Roeloffs 1988).

### 5.1 *Spatial points considered for the calculations*

A part of the normal fault is shown in figure 3 in projection on a vertical plane containing the $z$-axis.

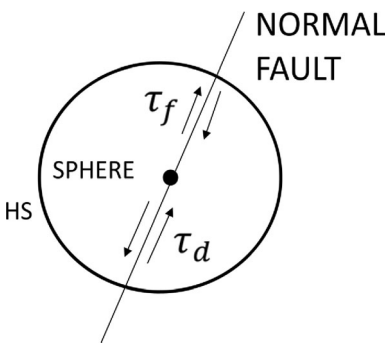


Figure 2. A normal fault intersecting the spherical inclusion. The destabilizing shear stress $(\tau_d)$ and the stabilizing frictional stress $(\tau_f)$ on the fault are also shown schematically.

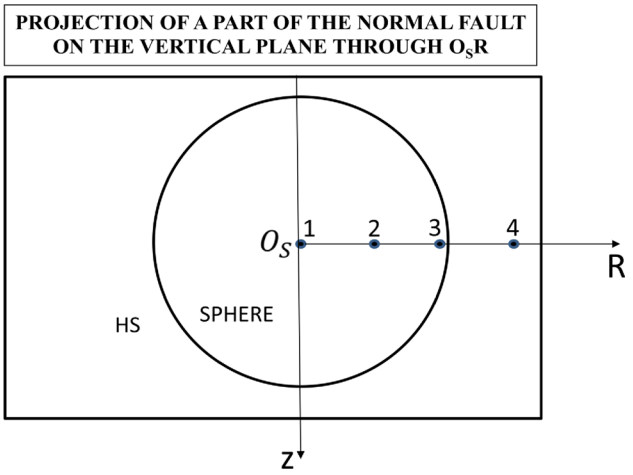


Figure 3. Another view of the fault and the sphere. See section 5.1 of the text for a detailed description.

The line $O_S R$ is a strike line of the fault. It is also the $\theta = 90°$ radial line of the spherical coordinate system. The spatial points considered for the following results are shown schematically as Points 1 to 4. Coordinates of Points 1–3 in the sphere are (0.1 m, 90°), (75 m, 90°) and (149.9 m, 90°), respectively. Point 1 is close to the center of the sphere rather than the center itself for mathematical reasons (equation A1c of Appendix A). Point 3 lies just inside the boundary of the sphere. The coordinates of Point 4 in the HS are (200 m, 90°).

### 5.2 *Numerical values of data used in calculations*

Values of the moduli (short for porous-elastic moduli) used during the calculations are given in table 1. They are based on values for different rock types given by Wang (2000, p266). All the values for HS are in the nominal range. Values for shear modulus ($G$) and Skempton's coefficient ($B$) for the sphere are also nominal. Value adopted for diffusivity ($c_S$) in the sphere is near but within the lower limit of the experimentally observed range. Values of undrained ($\nu_{uS}$) and drained ($\nu_S$) Poisson's ratios listed in column 3 of table 1 have been arrived at through calculations. Subscripts $S$ and $H$ indicate whether the moduli pertain to the sphere or the HS, respectively.

The adopted values of the radii of the sphere and the reservoir are 150 m and 1500 m, respectively. The results shown in table 1 are for a unit total weight of the reservoir. Values of some other parameters required for computations are given in Appendix B.

Table 1. *Values used for moduli.*

| Moduli | HS | Sphere |
|---|---|---|
| G (GPa) | 12.0 | 12.0 |
| $c$ (m$^2$ s$^{-1}$) | $5.0 \times 10^{-3}$ | $3.0 \times 10^{-5}$ |
| $B$ | 0.50 | 0.6 |
| $\nu_u$ | 0.35 | 0.1 – 0.30 |
| $\nu$ | 0.25 | $\nu_u$ – 0.01 |

### 5.3 *Reservoir influence at Point 1*

Table 2 provides a summary of results for reservoir influence at Point 1 of figure 3 for 10 different values of $\nu_{uS}$. It may be concluded from this table that, for the above adopted values of other moduli, if the value of $\nu_{uS}$ is greater than about 0.21, the magnitude of $\tau_d$ will be greater than that of $\tau_f$ and its phase will be near 0°. Thus, the reservoir influence will promote slip on the fault at Point 1 at or near peak water level.

If the value of $\nu_{uS}$ is between 0.21 and 0.18, the magnitude of $\tau_d$ will be less than that of $\tau_f$ and the reservoir influence will induce stability on the normal fault at Point 1.

Lastly, if the value of $\nu_{uS}$ is 0.17 or less, the magnitude of $\tau_d$ will be greater than that of $\tau_f$ and its phase will be close to 180°. The reservoir will promote slip on the fault at Point 1 at or near minimum water level.

### 5.4 *Reservoir influence at Points 1–3*

Table 3 lists results for Points 1, 2 and 3 (figure 3) in the sphere for $\nu_{uS}$ equal to 0.1. It follows from these results that reservoir influence will promote

Table 2. *Reservoir influence at Point 1 for 10 different values of $\nu_{uS}$.*

| | $\tau_f$ | | $\tau_d$ | |
|---|---|---|---|---|
| $\nu_{uS}$ | Mag. (Pa) | Phase | Mag. (Pa) | Phase |
| 0.30 | $1.12 \times 10^{-9}$ | 0.1° | $9.34 \times 10^{-9}$ | 0.1° |
| 0.25 | $1.87 \times 10^{-9}$ | −0.0° | $5.73 \times 10^{-9}$ | 0.3° |
| 0.22 | $1.47 \times 10^{-9}$ | −0.1° | $2.80 \times 10^{-9}$ | 0.7° |
| 0.21 | $2.70 \times 10^{-9}$ | −0.1° | $1.65 \times 10^{-9}$ | 1.4° |
| 0.20 | $2.96 \times 10^{-9}$ | −0.1° | $3.86 \times 10^{-10}$ | 6.6° |
| 0.19 | $3.25 \times 10^{-9}$ | −0.1° | $1.01 \times 10^{-9}$ | 177.2° |
| 0.18 | $3.57 \times 10^{-9}$ | −0.2° | $2.55 \times 10^{-9}$ | 178.7° |
| 0.17 | $3.92 \times 10^{-9}$ | −0.2° | $4.27 \times 10^{-9}$ | 179.1° |
| 0.15 | $4.76 \times 10^{-9}$ | −0.2° | $8.35 \times 10^{-9}$ | 179.4° |
| 0.10 | $8.21 \times 10^{-9}$ | −0.4° | $2.52 \times 10^{-8}$ | 179.4° |

Table 3. *Reservoir influence at Points 1–3 in the same sphere.*

| | $\tau_f$ | | $\tau_d$ | |
|---|---|---|---|---|
| $(R, 90°)$ | Mag. (Pa) | Phase | Mag. (Pa) | Phase |
| 0.1 m | $8.21 \times 10^{-9}$ | $-0.4°$ | $2.52 \times 10^{-8}$ | $179.4°$ |
| 75 m | $7.94 \times 10^{-9}$ | $0.3°$ | $2.52 \times 10^{-8}$ | $179.4°$ |
| 149.9 m | $1.33 \times 10^{-8}$ | $-0.5°$ | $2.51 \times 10^{-8}$ | $179.4°$ |

slip on the fault at minimum water level throughout the sphere.

### 5.5 *Reservoir influence at Point 4 in HS*

Computed results for the Point 4 (figure 3) in the HS are given in table 4 for moduli listed in column 2 of table 1. The listed, near zero, phase of $\tau_d$ indicates that the reservoir influence in this case will promote slip on the fault at peak reservoir level.

### 5.6 *Simulating a homogeneous HS with the three-dimensional model*

In another set of computations, we assumed that the sphere and the HS had identical moduli. In other words, we effectively considered reservoir influence on a normal fault in a homogeneous HS. But we followed the same calculation procedure as for the above results. It turned out that the reservoir influence would promote slip on the fault at peak reservoir level whatever value is assigned to $\nu_{uS}$. This result is discussed further in section 6.4.

## 6. Discussion

### 6.1 *Occurrence of normal fault earthquakes at low reservoir level*

We note on the basis of various sets of computations similar to those used to obtain the data shown in table 2 that the values of $\nu_{uS}$ at which the transitions from reservoir promoted instability to stability and then instability again take place depend upon values adopted for other moduli also. But, in every case, a low value of $\nu_{uS}$ is required for promotion of slip on the subsurface fault at Point 1 at low reservoir level.

Thus, one possible explanation for the occurrence of a normal fault earthquake at low reservoir level could be that its hypocenter was located in a small rock volume with low diffusivity and low undrained and drained Poisson's ratios. Similarly, an earthquake under the same reservoir at peak water level could have its hypocenter on the fault outside the rock volume.

Table 4. *Reservoir influence at Point 4 in the HS.*

| | Mag. (Pa) | Phase |
|---|---|---|
| $\tau_f$ | $1.13 \times 10^{-9}$ | $-0.4°$ |
| $\tau_d$ | $1.18 \times 10^{-8}$ | $-0.1°$ |

### 6.2 *The moduli*

Roeloffs (1988) considered a two-dimensional model involving a reservoir of infinite length in one horizontal direction resting on a uniform PE half space to explain post-impoundment normal fault earthquakes under Lake Mead. Relatively low values of the moduli for the half space were required to explain such earthquakes. These included: $B = 0.106, \nu_u = 0.206$ and $\nu = 0.200$. Value of $c$ was not stated explicitly. But Westerly Granite was one of the rocks considered. Wang (2000) lists a value of $c = 2.2 \times 10^{-5}$ m$^2$ s$^{-1}$ for this rock.

The values of moduli used for the above results are listed in table 1 and the first column of table 2. Briefly, comparably low values of $c_S$, $\nu_{uS}$ and $\nu_S$ are required with our model also.

Thus, low values of some moduli are required to explain the occurrence of normal fault earthquakes at minimum reservoir level in Roeloffs (1988) model as well as the present model. The rock with such anomalous values occupies an entire half space in the former case and a sphere of small radius in the latter case (see second paragraph of section 2).

### 6.3 *Dip of the normal fault*

Rogers and Lee (1976, table 3) had estimated a dip of 50° from their composite fault-plane solutions for normal faults under Lake Mead. Our calculated results and conclusions for a fault dip of 50° are similar to those presented above for a fault with a dip of 60°.

### 6.4 *Influence of the shape of the reservoir*

The results of section 5.6 above indicate that a uniform circular reservoir resting on a homogeneous HS favours normal fault earthquakes at peak reservoir level only. Roeloffs (1988) showed that an

infinitely long reservoir can favour earthquakes at different phases of reservoir cycle depending on the moduli of the HS.

This reiterates that the shape, size and uniformity of the bottom of the reservoir influence the response of the buried fault.

### 6.5 *Importance of ambient tectonic stresses in promoting post-impoundment earthquakes*

The role of reservoir influence in promoting post-impoundment earthquakes has been considered above in considerable detail. But the role of ambient tectonic stresses is crucial also in the occurrence of reservoir 'promoted' earthquakes (Chander and Kalpna 1997). There are two requirements. First, the influence of the reservoir and the tectonic forces must be separately such that the destabilizing shear stress exceeds the stabilizing frictional stress on the subsurface fault. Second, the total combined destabilizing shear stress must exceed the total combined stabilizing frictional stress on the fault. Routine pre-impoundment site investigations do not include adequate measurements of ambient tectonic stresses.

### 6.6 *Non-uniqueness*

The foregoing interpretation of observations of post-impoundment normal fault earthquakes is non-unique because the considered model is not based on any site-specific investigations of the subsurface.

## 7. Conclusion

The above numerical results and analysis reveal how a reservoir may influence slip on a normal fault passing through a small rock volume with significantly lower values of diffusivity, and undrained and drained Poisson's ratios than those of the other rocks at the site. At points of the fault within the rock volume, the reservoir will promote slip at low water level. On the other hand, at points of the fault outside the rock volume, the reservoir will promote slip at maximum water level.

## Acknowledgement

We are grateful to Prof S J Singh for reading an early draft of Appendix A.

## Appendix A

### Estimation of the reservoir-induced destabilizing shear stress and stabilizing frictional stresses on a steeply dipping normal fault using the selected three-dimensional model of the subsurface

#### A1. *Preliminaries*

A1.1 *Review:* The following procedure has been evolved by us. Still, we recall for a perspective that a sphere or a spherical cavity has been considered in several earlier studies of elastic and porous-elastic media. Thus, to simulate elastic waves from a nuclear explosion, Thiruvenkatachar and Viswanathan (1965) investigated the dynamic response of an elastic half space to time dependent surface tractions acting on an embedded spherical cavity. Datta (1969) considered a rigid spherical inclusion in an elastic half space and obtained results for small vertical vibrations of the center of the sphere. The mathematical iterative approach was identical in both these articles.

Thermo-elastodynamic response of a spherical cavity in a saturated porous-elastic medium was investigated by Ganbi *et al.* (2010). He and Jin (2011) considered effects of a local heat source on the pore pressure and thermal stresses around a spherical cavity in a porous medium. Bai and Li (2013) examined the irreversible consolidation problem of a saturated porothermoelastic (sic) spherical body with a spherical cavity.

Our problem is intermediate between these two sets of sphere or spherical cavity problems. Consideration of a porous-elastic medium is more complex than consideration of a purely elastic medium, but consideration also of thermal effects in the porous-elastic medium is not necessary for our purpose.

A1.2. *An approximation:* Among the possible physical fields that may permeate a porous-elastic solid, our interest is in stress, displacement and pore pressure fields (SDPFs for short). Both the reservoir and the sphere exert influence on the SDPFs in the HS. In turn, the SDPFs in the sphere have contributions due to the reservoir as well as due to the presence of the sphere itself within the HS. Thiruvenkatachar and Viswanathan (1965) acknowledged that, in their case, the elastic stress and displacement fields in the elastic half space were influenced by the presence of the spherical cavity.

But we consider only those fields in the sphere and HS that are due to direct influence of the reservoir. In order to increase the precision of the numerical results obtained with this approximation, the radius of the sphere is kept small compared to the depth of its center and the radius of the reservoir.

A2. *SDPFs referred to cylindrical coordinates*

The elements of stress, displacement and pore pressure fields (SDPFs) in a PE solid using the cylindrical coordinate system of figure 1 are $\sigma_{zz}, \tau_{rz}, \sigma_{rr}, u_r, u_z$ and $p$. The following expressions for these SDPFs are taken from equations (9.47, 9.48, 9.42, 9.46 and 9.51) of Wang (2000). The expression for $\sigma_{rr}$ in equation (A1c) below was derived by us.

$$\begin{aligned}\sigma_{zz}(r,z) = 2G\int_0^\infty \Big\{ &\frac{k^2\gamma c}{\iota\omega}(A_{1k}e^{mz} + A_{2k}e^{-mz}) \\ &- (a_1 kz - a_4)A_{3k}e^{kz} \\ &+ (a_1 kz + a_4)A_{4k}e^{-kz} - k(A_{5k}e^{kz} \\ &+ A_{6k}e^{-kz})\Big\} kJ_0(kr)\,dk; \end{aligned} \tag{A1a}$$

$$\begin{aligned}\tau_{rz}(r,z) = 2G\int_0^\infty \Big\{ &\frac{-km\gamma c}{\iota\omega}(A_{1k}e^{mz} - A_{2k}e^{-mz}) \\ &+ (a_1 kz - 0.5)A_{3k}e^{kz} + (a_1 kz + 0.5)A_{4k}e^{-kz} \\ &+ k(A_{5k}e^{kz} - A_{6k}e^{-kz})\Big\} kJ_1(kr)\,dk; \end{aligned} \tag{A1b}$$

$$\begin{aligned}\sigma_{rr}(r,z) = 2G\int_0^\infty \Big\{ &\left(\frac{k^2\gamma c}{\iota\omega} - \gamma\right)(A_{1k}e^{mz} - A_{2k}e^{-mz}) \\ &+ a_1(kz + 2\nu_u)A_{3k}e^{kz} \\ &+ a_1(-kz + 2\nu_u)A_{4k}e^{-kz} \\ &+ k(A_{5k}e^{kz} + A_{6k}e^{-kz})\Big\} kJ_0(kr)\,dk \\ &- \frac{2G}{r}\int_0^\infty \Big\{ \frac{k\gamma c}{\iota\omega}(A_{1k}e^{mz} + A_{2k}e^{-mz}) \\ &+ a_1 z(A_{3k}e^{kz} - A_{4k}e^{-kz}) \\ &+ A_{5k}e^{kz} + A_{6k}e^{-kz}\Big\} kJ_1(kr)\,dk; \end{aligned} \tag{A1c}$$

$$\begin{aligned}u_r(r,z) = \int_0^\infty \Big\{ &\frac{-k\gamma c}{\iota\omega}(A_{1k}e^{mz} + A_{2k}e^{-mz}) \\ &+ a_1 z(A_{3k}e^{kz} - A_{4k}e^{-kz}) \\ &+ k(A_{5k}e^{kz} + A_{6k}e^{-kz})\Big\} kJ_1(kr)\,dk; \end{aligned} \tag{A1d}$$

$$\begin{aligned}u_z(r,z) = \int_0^\infty \Big\{ &\frac{m\gamma c}{\iota\omega}(A_{1k}e^{mz} - A_{2k}e^{-mz}) \\ &- (a_1 z - a_2/k)A_{3k}e^{kz} \\ &- (a_1 z + a_2/k)A_{4k}e^{-kz} \\ &- k(A_{5k}e^{kz} - A_{6k}e^{-kz})\Big\} kJ_0(kr)\,dk; \end{aligned} \tag{A1e}$$

$$\begin{aligned}p_l(r,z) = 2\gamma G\int_0^\infty \Big\{ &a_5(A_{1k}e^{mz} + A_{2k}e^{-mz}) \\ &- a_4(A_{3k}e^{kz} + A_{4k}e^{-kz})\Big\} kJ_0(kr)\,dk; \end{aligned} \tag{A1f}$$

In these equations,

$$\begin{aligned} a_1 &= 1/(2(1-2\nu_u)); \\ a_2 &= (3-4\nu_u)a_1; \\ a_4 &= 2(1-\nu_u)a_1; \\ m &= \sqrt{k^2 + \iota\omega/c}; \\ a_5 &= B(1-\nu)(1+\nu_u)/(3(\nu_u-\nu)); \\ \gamma &= B(1+\nu_u)/(3(1-\nu_u)). \end{aligned}$$

Let $U_{iS}(r,z)$ and $U_{iH}(r,z)$, $i = 1,\ldots,6$, represent $\sigma_{zz}, \tau_{rz}, \sigma_{rr}, u_r, u_z$ and $p$ in the sphere and the HS. Since each of the above equations contains the same six unknown constants $A_{jk}$ with different multiplying factors, therefore equations (A1a–A1f) for the sphere and the HS can be written compactly as follows:

$$U_{iS}(r,z) = \int_0^\infty U'_{iS}(k,r,z)\,dk, \quad (i = 1,\ldots,6), \tag{A2a}$$

$$U_{iH}(r,z) = \int_0^\infty U'_{iH}(k,r,z)\,dk, \quad (i = 1,\ldots,6). \tag{A2b}$$

The abbreviated expressions for the integrands are:

$$U'_{iS}(k,r,z) = \sum_{j=1}^{6} \alpha'_{ijS}(k,r,z)A_{jkS}, \quad (i = 1,\ldots,6), \tag{A3a}$$

$$U'_{iH}(k,r,z) = \sum_{j=2,4,6} \alpha'_{ijH}(k,r,z)A_{jkH}, \quad (i = 1,\ldots,6). \tag{A3b}$$

Only terms with negative exponentials are retained in the case of the HS to ensure finiteness of fields as $z$ tends to infinity.

The coordinates $(r, z)$ and $(R, \theta)$ for a given point in the space portrayed in figure 1 are related as follows:

$$r = R\sin\theta; \quad z = z_0 - R\cos\theta.$$

Therefore, through these substitutions, we may write the above equations also as:

$$U_{iS}(R,\theta) = \int_0^\infty U'_{iS}(k,R,\theta)\,dk, \quad (i = 1,\ldots,6), \tag{A4a}$$

$$U_{iH}(R,\theta) = \int_0^\infty U'_{iH}(k,R,\theta)\,dk, \quad (i = 1,\ldots,6). \tag{A4b}$$

$$U'_{iS}(k,R,\theta) = \sum_{j=1}^{6} \alpha'_{ijS}(k,R,\theta)A_{jkS}, \quad (i = 1,\ldots,6). \tag{A5a}$$

$$U'_{iH}(k,R,\theta) = \sum_{j=2,4,6} \alpha'_{ijH}(k,R,\theta)A_{jkH}, \quad (i = 1,\ldots,6). \tag{A5b}$$

## A3. *SDPF elements for spherical coordinates*

The spherical elements $\sigma_{RR}, \tau_{R\theta}, u_\theta, u_R$, $p$ and $\partial p/\partial R$ of SDPFs are related to the above cylindrical elements for the sphere and the HS through the following equations.

$$\sigma_{RR}(R,\theta) = U_1(R,\theta)\cos^2\theta - U_2(R,\theta)\sin 2\theta + U_3(R,\theta)\sin^2\theta, \tag{A6a}$$

$$\tau_{R\theta}(R,\theta) = [U_1(R,\theta) - U_3(R,\theta)]\sin\theta\cos\theta + U_2(R,\theta)\cos 2\theta, \tag{A6b}$$

$$u_\theta(R,\theta) = U_4(R,\theta)\cos\theta + U_5(R,\theta)\sin\theta, \tag{A6c}$$

$$u_R(R,\theta) = U_4(R,\theta)\sin\theta - U_5(R,\theta)\cos\theta, \tag{A6d}$$

$$p(R,\theta) = U_6(R,\theta). \tag{A6e}$$

The quantity $\partial p/\partial R$ is obtained by straight forward differentiation of equation (A6e).

Let $V_{iS}(R,\theta)$ and $V_{iH}(R,\theta)$, $(i = 1,\ldots,6)$, represent $\sigma_{RR}, \tau_{R\theta}, u_R, u_\theta, p$ and $\partial p/\partial R$ in the sphere and the HS. Then,

$$V_{iS}(R,\theta) = \int_0^\infty V'_{iS}(k,R,\theta)\,dk, \quad (i = 1,\ldots,6), \tag{A7a}$$

$$V_{iH}(R,\theta) = \int_0^\infty V'_{iH}(k,R,\theta)\,dk, \quad (i = 1,\ldots,6). \tag{A7b}$$

The integrands take the form:

$$V'_{iS}(k,R,\theta) = \sum_{j=1}^{6} \beta'_{ijS}(k,R,\theta)A_{jkS}, \quad (i = 1,\ldots,6), \tag{A8a}$$

$$V'_{iH}(k,R,\theta) = \sum_{j=2,4,6} \beta'_{ijH}(k,R,\theta)A_{jkH}, \quad (i = 1,\ldots,6). \tag{A8b}$$

The $\beta'_{ij}$'s for each $j$ between 1 and 6 are obtained from the corresponding $\alpha'_{ij}$'s using equations (A6a–A6e). We emphasize that the unknown constants $A_{jkS}$, $j = 1,\ldots,6$ in equations (A3a, A5a and A8a) are the same respectively and the unknown constants $A_{jkH}$, $j = 2, 4, 6$ in equations (A3b, A5b and A8b) are the same similarly. This is useful for solving the problem.

## A4. *Evaluation of unknown constants for the HS*

Following the approximation stated in section A1.2 above, we proceed as if the HS is homogeneous. We consider that the top surface is pervious. Therefore, boundary conditions on $\sigma_{zzH}, \tau_{rzH}$ and $p_H$ are pertinent here. The following three equations are obtained from equations (A1a, A1b and A1f) by setting $z = 0$. In these equations, $J_1(R_R k)/(\pi R_R k)$ and $-J_1(R_R k)/(\pi R_R k)$ represent, in the $k$-domain, the vertical normal stress and pore pressure exerted on the surface of the HS by a uniform circular water reservoir of radius $R_R$ and unit total weight.

$$2G_H\left[\frac{k^2\gamma_H c_H}{\iota\omega}A_{2kH} + a_{4H}A_{4kH} - kA_{6kH}\right] = \frac{J_1(R_R k)}{\pi R_R k},$$

$$2G_H\left[\frac{km_H\gamma_H c_H}{\iota\omega}A_{2kH} + 0.5A_{4kH} - kA_{6kH}\right] = 0,$$

$$2\gamma_H G_H[a_{5H}A_{2kH} - a_{4H}A_{4kH}] = -\frac{J_1(R_R k)}{\pi R_R k}.$$

With $A_{jkH}$ $(j = 2, 4, 6)$, determined from the above equations, the right-hand sides of all the expressions in equations (A3b, A5b and A8b) can be evaluated.

A5. *Evaluation of unknown constants for the sphere*

A5.1 *Boundary conditions on the surface of the sphere:* The boundary conditions on the interface between the sphere and the HS are obtained from equations (A3a and A3b) with $R = R_S$, where $R_S$ is the radius of the sphere:

$$V_{iS}(R_S, \theta) = V_{iH}(R_S, \theta), \quad i = 1, \ldots, 6, \quad 0 \le \theta \le \pi. \tag{A9a}$$

These conditions also hold for each $k$. Thus, from equations (A5a and A5b)

$$V'_{ikS}(k, R_S, \theta) = V'_{ikH}(k, R_S, \theta), \quad i = 1, \ldots, 6, \quad 0 \le \theta \le \pi. \tag{A9b}$$

These equations may be rewritten using equations (A8a) as:

$$\sum_{j=1}^{6} \beta'_{ijS}(k, R_S, \theta) A_{jkS} = V'_{ikH}(k, R_S, \theta), \quad i = 1, \ldots, 6, \quad 0 \le \theta \le \pi. \tag{A9c}$$

A5.2 *Finite cosine transform:* Use of finite cosine transform (FCT) technique is convenient to apply these point-wise conditions on the spherical boundary. Sneddon (1951, p72) gives the following relations for FCT and its inverse. If $0 \le \theta \le \pi$, then

$$f'(n) = \int_0^{\pi} f(\theta) \cos n\theta \; d\theta, \tag{A10a}$$

$$f(\theta) = \frac{1}{\pi} f'(0) + \frac{2}{\pi} \sum_{n=1}^{\infty} f'(n) \cos n\theta. \tag{A10b}$$

A5.2.1 *Use of FCT:* Applying equation (A10a) on both sides of equations (A9c), we have:

$$\beta''_{ijS}(k, R_S, n) = \int_0^{\pi} \beta'_{ijS}(k, R_S, \theta) \cos n\theta \; d\theta, \quad i, j = 1, \ldots, 6, \; n = 0, \ldots, N, \tag{B8a}$$

$$V''_{iH}(k, R_S, n) = \int_0^{\pi} V'_{iH}(k, R_S, \theta) \cos n\theta \; d\theta, \quad i = 1, \ldots, 6, \; n = 0, \ldots, N. \tag{B8b}$$

Thus, the equations (A9c) take the following form in the FCT domain.

$$\sum_{j=1}^{6} \beta''_{ijS}(k, R_S, n) A_{jknS} = V''_{iH}(k, R_S, n), \quad i = 1, \ldots, 6, \quad n = 0, \ldots, N.$$

On solving these equations for each $n$ in the range $n = 0, \ldots, N$, we obtain $N + 1$ sets of values of the $A_{jknS}$, $j = 1, \ldots, 6$ for one value of $k$. The FCT integral are computed numerically.

A6. *Determination of SDPFs at a point in the sphere*

In order to compute reservoir influence at a point $(R, \theta)$ within the sphere, we obtain the following equivalents of equations (A5a) in the FCT domain:

$$U''_{ikS}(k, R_1, n) = \sum_{j=1}^{6} \alpha''_{ijS}(k, R_1, n) A_{jknS}, \quad i = 1, \ldots, 6, n = 0, \ldots, N,$$

$\alpha''_{ijS}(k, R_1, n)$ on the right-hand side can be computed. Therefore, using $A_{jknS}$'s determined in the section A5.4, the summands on the right-hand sides in these equations can be evaluated. Thus, the left-hand sides of these equations are evaluated also.

The inverse finite cosine transform defined in equation (A10b) then allows us to obtain for each $i = 1, \ldots, 6$,

$$U'_{ikS}(k, R, \theta) \approx \frac{1}{\pi} U''_{ikS}(k, R, 0) + \frac{2}{\pi} \sum_{n=1}^{N} U''_{ikS}(k, R, n) \cos n\theta.$$

The approximate equality symbol is used because the infinite series given in equation (A10a) has been curtailed to a $N$ term series. The above entire procedure has to be repeated for suitably large number of values of $k$ so that integrations with respect to $k$ in equations (A5a) may be carried out numerically to obtain the values of $U_{iS}(R, \theta)$.

A7. *Computation of $\tau_d$ and $\tau_f$*

The expressions for $\tau_d$ and $\tau_f$ at a point $(R, \theta)$ on the fault within the sphere or the HS in terms of respective $U_i(R, \theta)$, $i = 1, \ldots, 6$ are as follows.

$$\tau_d(R,\theta) = [U_1(R,\theta) - U_3(R,\theta)]\sin\delta\cos\delta + U_2(R,\theta)\cos 2\delta;$$
$$\tau_f(R,\theta) = \mu[\sigma(R,\theta) - U_6(R,\theta)];$$
$$\sigma(R,\theta) = U_1(R,\theta)\cos^2\delta - U_2(R,\theta)\sin 2\delta + U_3(R,\theta)\sin^2\delta.$$

A computer program was written for calculating $\tau_d$ and $\tau_f$.

## Appendix B

The following abbreviations and symbols are used in the text and Appendix A for brevity and specificness.

### Abbreviations

| | |
|---|---|
| moduli | Porous-elastic moduli |
| sphere | Porous-elastic sphere |
| FCT | Finite cosine transform |
| HS | Porous-elastic half space of the three-dimensional model |
| PE | Porous-elastic |
| SDPFs | Stress, displacement and pore pressure fields |
| $U$ | SDPFs $\sigma_{zz}$, $\tau_{rz}$, etc. |
| $V$ | SDPFs $\sigma_{RR}$, $\tau_{R\theta}$, etc. |

### Symbols

| | |
|---|---|
| $c$ | Hydraulic diffusivity |
| $\iota$ | Used with the imaginary parts of complex variables |
| $k$ | Hankel transform variable |
| $n$ | Finite cosine transform variable |
| $p$ | Pore pressure |
| $r$ | Radial coordinate in the cylindrical system |
| $zz$ | Coordinate in the cylindrical system |
| $A$ | Unknown constants to be determined from boundary conditions |
| $B$ | Skempton's coefficient |
| $G$ | Shear Modulus |
| $J$ | Bessel Function |
| $O$ | Origin of a coordinate system |
| $R$ | Radial coordinate in the spherical system |
| $\alpha$ | Coefficient of $A$ in equations (A3a, A3b, A5a, A5b) |
| $\beta$ | Coefficient of $A$ in equations (A7a, A7b) |
| $\gamma$ | Loading efficiency |
| $\delta$ | Dip of fault plane |
| $\theta$ | Angle measure in the spherical system |
| $\mu$ | Coefficient of rock friction |
| $\nu$ | Poisson's ratio |
| $\sigma$ | Normal stress |
| $\tau$ | Shear stress |
| $\omega$ | Angular frequency |

### Subscript

| | |
|---|---|
| $d$ | Destabilizing stress |
| $f$ | Frictional stress |
| $i$ | Running index for $i = 1, \ldots, 6$ |
| $j$ | Running index for $j = 1, \ldots, 6$ |
| $k$ | Value in $k$ domain |
| $u$ | Undrained Poisson's ratio |
| $H$ | Variables in HS |
| $S$ | Variable in sphere |

### Superscripts

| | |
|---|---|
| $'$ | Hankel transform of the variable |
| $''$ | Finite cosine transform of the variable |

### Numerical values of some variables used in all computations

$z_0 = 5000$ m,
$R_R = 1500$ m,
$R_S = 150$ m,
$\mu = 0.6$,
$\omega = 2 \times 10^{-7}$ radians s$^{-1}$.

### References

Bell M L and Nur A 1978 Strength changes due to reservoir-induced stresses and pressure and application to Lake Oroville; *J. Geophys. Res.* **83** 4469–4483.

Bai B and Li T 2013 Irreversible consolidation problem of a saturated porothermoelastic spherical body with spherical cavity; *Appl. Math. Model.* **37** 1973–1982.

Chander R and Tomar S K 2016 On a model simulating lack of hydraulic connection between a man-made reservoir and the volume of poroelastic rock hosting a post-impoundment earthquake; *J. Earth Syst. Sci.* **125** 1543–1556.

Chander R and Kalpna 1997 On categorising induced and natural tectonic earthquakes near new reservoirs; *Eng. Geol.* **46** 81–92.

Datta S K 1969 An axisymmetric problem of an elastic half space containing a rigid inclusion; *Quart. J. Mech. Appl. Math.* **XXII** 439–451.

Gupta H K and Rastogi B K 1976 *Dams and Earthquakes;* Elsevier, Amsterdam, 229p.

Jaeger J C and Cook N G W 1969 *Fundamentals of Rock Mechanics;* Methuen, London, 515p.

Liu Ganbi, Xie Kanghe and Zheng Rongue 2010 Thermoelastodynamic response of a spherical cavity in a saturated poroelastic medium; *Appl. Math. Model.* **34** 2203–2222.

He L-W and Jin Z-H 2011 Effects of local thermal non-equilibrium on the pore pressure and thermal stresses around a spherical cavity in a porous medium; *Int. J. Eng. Sci.* **49** 240–252.

Rogers A M and Lee W H K 1976 Seismic study of earthquakes in Lake Mead, Nevada–Arizona Region; *Bull. Seismol. Soc. Am.* **66** 1667–1681.

Roeloffs E A 1988 Fault stability changes induced beneath a reservoir with cyclic variations in water level; *J. Geophys. Res.* **91** 2107–2124.

Segall P 1985 Stress and subsidence resulting from subsurface fluid withdrawal in the epicentral region of the 1983 Coalinga earthquake; *J. Geophys. Res.* **90** 6801–6816.

Singh S J and Rani S 2006 Plane strain deformation of a multilayered poroelastic half space; *J. Earth Syst. Sci.* **115** 685–694.

Snow D T 1972 Geodynamics of seismic reservoirs; *Proc. Flow Fractured Rock, German Soc. Soil Rock Mech.* T2-J; 1–9.

Sneddon I N 1951 *Fourier Transforms.* McGraw-Hill Book Company Inc, New York, 541p.

Thiruvenkatachar V R and Viswanathan K 1965 Dynamic response of an elastic solid half-space to time-dependent surface tractions over an embedded spherical cavity; *Proc. Roy. Soc.* **A287** 549–567.

Wang H F 2000 *Theory of Linear Poroelasticity with Applications to Geomechanics and Hydrogeology;* Princeton University Press, Princeton, New Jersey, 287p.

Corresponding editor: Munukutla Radhakrishna